ORIGINAL ARTICLE

Kinetic and isotherm studies of Acid Orange 7 dye absorption using sulphonated mandarin biochar treated with TETA

Ahmed Eleryan[1] · Mohamed A. Hassaan[1] · Uyiosa O. Aigbe[2] · Kingsley E. Ukhurebor[3] · Robert B. Onyancha[4] · Mohamed A. El-Nemr[5] · Safaa Ragab[1] · Ismail Hossain[6] · Ahmed El Nemr[1]

Abstract

This study contributes to the current state of knowledge by highlighting the physical–chemical interactions between biochar and dyes. The removal of Acid Orange 7 (AO7) dye by a modified biochar obtained from the wastes of mandarin peels (MPs) has been investigated in this work. A dehydration procedure with 80% H_2SO_4 under reflux was applied to produce an innovative biochar from MPs and then boiled with H_2O_2 and followed by boiling with triethylenetetramine to make mandarin biochar-C-TETA (MBCT). FTIR, SEM, EDX, BJH, BET, TGA, and DTA analyses were applied to investigate the MBCT. FTIR analysis showed an additional peak that confirmed the addition of the NH_2 group to the MBCT structure. An amorphous carbon structure was also confirmed by XRD analysis. The AO7 dye solution pH was proved to give the best absorption at pH 2.0. Significant removal of AO7 dye 99.07% using an initial concentration of 100 mg/L of AO7 dye and a 0.75 g/L MBCT. The Langmuir (LNR) and Freundlich (FRH) isotherm models investigated the experimental results. The LNR was best suited to handle the working MBCT data. The maximum adsorption capacity (Q_m) calculated for the MBCT was 312.5 mg/g using 0.25 g/L of the MBCT. Kinetic studies were conducted using the intraparticle diffusion (IND), film diffusion (FD), pseudo-first-order (PFOR), and pseudo-second-order (PSOR) models. The absorption rate was calculated using the ultimate value of the linear regression coefficient ($R^2 > 0.99$), and the PSOR rate model was found to ideally describe the absorption process. The point of zero charge (pHPZC) was found to be 10.17. The electrostatic attractive-forces between the sorbent surface positively charged sites and negatively charged anionic dye molecules were the primary mechanism of the MBCT sorption of the AO7 dye's anion absorption. The results indicate that the manufactured MBCT adsorbent may be useful for removing the AO7 dye from wastewater. MBCT can be used repeatedly for up to six cycles without dropping its absorption efficiency.

Keywords Absorption · Acid Orange 7 dye · Mandarin peels · Agricultural wastes · Aquatic environments · Removal of dye

Highlights
- The LNR and PSOR are best fitted for the AO7 dye absorption by MBCT.
- MBCT is an operative and inexpensive sorbent for AO7 dye absorption.
- The MBCT maximum absorption capacity (Q_m) of AO7 dye is 312.5 mg/g.
- A highly acidic medium is the ideal pH value (2.0) for AO7 dye absorption.

✉ Ahmed El Nemr
   ahmedmoustafaelnemr@yahoo.com;
   ahmed.m.elnemr@gmail.com

Extended author information available on the last page of the article

1 Introduction

The rapid and ongoing industrial growth that results from the expanding global population has several negative effects, most notably environmental pollution [1]. More than one million tons of dye are produced annually universal for use in various industries, particularly the textile industry, which is the world's second-largest end user of freshwater [2, 3]. Dye wastewater is generated or used in many different manufacturing industries, including the paper and tannery industries, the pharmaceutical, food, and cosmetics industries, as well as the textile and dyeing industries [4, 5].

Synthetic dyes are one of the particular toxins that pollute the environment nowadays [6–8]. The majority of dyes, notably azo dyes, are highly stable to sunlight and have

complex aromatic, poisonous, mutagenic, and carcinogenic structures [9–11]. As a result of the rising production of coloured products and their extensive usage in modern society, environmental researchers are extremely concerned about the development of coloured wastewater [11–13].

When water having azo dyes is discharged, it not only degrades the aesthetic appeal of receptor waters but also prevents sunlight from entering the body of water, inhibits photosynthesis, and lowers the concentration of dissolved oxygen. Twenty percent (one-fifth) of the colours applied in the textile sector are loosed into the environment untreated and slightly more than 10% of them enter wastewater [11]. One of the acidic azo dyes that harms the eyes and skin and is chronically toxic and carcinogenic is Acid Orange 7 (AO7) dye [11]. AO7 dye is also known as 2-naphthol orange (with a molecular formula of $C_{16}H_{11}N_2NaO_4S$ and its structure is shown in Fig. 1). It is generally utilized in the paper, textile dye industries, and food. It is also applied for the manufacture of personal care, washing agents, and laundry [14]. As a result, it is generally used to dye silk and wool. It is also frequently used to dye wool. It can also be used to colour leather, paper, and fabrics made of wool, silk, and polyamide fibres for direct printing. It can also be used as an indicator and for biological shading. Organic pigments contain heavy metal salt, which can be consumed as a food dye. It is made by azo coupling -naphthol with a diazonium derivative of sulfanilic acid [14].

Industries are now under enormous pressure from the public and convention rules to treat their wastewater favourably before releasing it into the ecosystem [15, 16]. Finding efficient treatment options is therefore essential and inevitable. So far, several procedures have been investigated for the dye absorption from wastewater, containing oxidation, anaerobic treatment, electrochemical coagulation methods, flotation, ion exchange, and chemical precipitation [11, 17]. In latest decades, the surface adsorption technique, which has straightforward and affordable mechanisms, has gained a lot of decades in the wastewater treatment industry [4, 18]. For the effi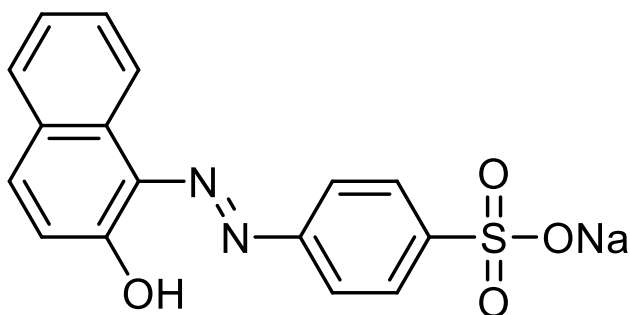cient absorption of soluble contaminants, especially organic compounds like paint, from water, this method frequently uses activated carbon (AC) or raw and inactivated biological materials like agricultural waste ash and bentonite [4, 11]. Some benefits of the surface adsorption process include its simple design, operation and low initial cost, the need for a lower energy source, and the deficiency of impact of toxic materials in the process. Researchers, however, have been forced to find solutions to these separation issues and modify the method of applying absorbents due to limitations in the surface absorption process, such as increased water suspended solids brought on by applications of powder forms and their challenging separation, particularly from the water environment [4, 6]. The utilization of cheap materials like agricultural residue for manufacture has also been highly considered as a potential solution to reduce preparation costs [4, 19].

While this is happening, employing food waste has been considered in various investigations since it lowers the cost of managing biomass, prevents the hygienic growth of the biological mass, and generates capital from agricultural and food wastes. Additionally, the AC made from agricultural and food waste has a low ash content, appropriate hardness, a high surface area, and a suitable porosity structure; for these reasons, their usage in the creation of bio-adsorbents has been taken into consideration [4, 6]. The effectiveness of peels from mandarins' residue as a granule in surface adsorption of AO7 dye from water solutions is investigated in this study for the 1st time because cellulosic residues are appropriate alternatives for creating adsorbents given the fundamental problem of powder adsorbent separation from the water body. The citrus fruit known as the mandarin belongs to the citrus family and can be found in temperate climates. According to numbers released in 2013, the FAO organization's data indicates that the annual production of mandarin oranges is roughly 21 million metric tons. China, Egypt, Turkey, Brazil, Spain, South Korea, Japan, and Italy have the highest production rates. Peels from mandarins used to make fruit juice make up about 8–14% of the total mass of the fruit and are discarded into the environment after use [19]. They are mostly utilized in the fuel, animal feed, and fertiliser industries and the cosmetics sector [4, 20]. A fruit peel sizable quantity is produced as biomass waste as a result of the extensive use of mandarins [19]. The composition of MPs contains organic substances, including cellulose, hemicellulose, and pectin, which makes it possible to pyrolyze the peel of the fruit to create biochar that is good for the environment. In this way, it is possible to generate materials with a high absorption capability [8, 19].

However, there has been little comprehensive research about the effect of the physio-chemical properties of biochar made from MPs on the absorption of dyes from aqueous solution [5]. As a potential substance for the AO7 dye absorption from wastewater, there haven't been any reported

Fig. 1 Molecular structure of AO7 dye (molecular formula: $C_{16}H_{11}N_2NaO_4S$) [14]

studies on the absorption efficiency of biochar made from MPs by dehydration with 80% H_2SO_4, then oxidation with H_2O_2, followed aminated via boiling with triethylenetetramine (TETA). Hence, this research work examined fabricated mandarin biochar-C-TETA (MBCT) for its effectiveness in exterminating the AO7 dye from water, which was produced using peels from mandarins' waste materials (a considerably cheaper agricultural waste product). FTIR, SEM, EDX, BET, BJH, TGA, and DTA analyses were used to characterize the prepared MBCT adsorbent. Variable parameters like the AO7 dye initial concentration, solution pH, time (duration) of the contact between the MBCT and the AO7 dye, and the impact of the MBCT dose were all investigated as part of the inquiry into the AO7 dye absorption conditions from water. To determine the absorption mechanism and the maximal adsorption capacity, the kinetic and isotherm models for AO7 dye absorption by MBCT were also examined. MBCT regeneration was also investigated from an economic point of view.

2 Materials and methods

2.1 Materials

Mandarin orange (*Citrus reticulata*) peels (MPs, waste material) obtained from a local market were applied to fabricate of MBCT. H_2SO_4 (99%), H_2O_2 (50%), TETA, and AO7 dye ($C_{16}H_{11}N_2NaO_4S$) were purchased from Sigma-Aldrich, Germany. Stock solution of AO7 dye was formed by adding 1 g to 1000 mL of distilled water (DW). A JSOS-500 shaker, a JENCO-6173 pH metre, and a digital UV/Visible spectrophotometer (SPEKOL1300) with glass cells and a 1-cm optical path were employed.

2.2 Preparation of MBCT

MPs were washed with DW, dried for 72 h at 120 °C, and then crushed and ground. Dried MPs (200 g) were boiled for 5 h in 1.0 L of 80% of H_2SO_4 in a refluxed system (300 °C), filtered and washed with DW until the filtrate became neutral, washed with ethanol, then dried for 24 at 120 °C, and weighed to produce 95 g. This type of preparation resulted in the sulphonation processes. As a result of this reaction, 90 g of the MPs biochar-based biosorbent were created, which were then suspended in 400 mL of 50% H_2O_2 and heated for 1 h at 100 °C. Filtered, washed with DW, and dried 24 h at 120 °C to get 80 g of the oxidized MPs biochar-CO-based biosorbent. A 150 mL of TETA was cooked for 4 h in a refluxed system with 50 g of the oxidized MPs biochar-CO-based biosorbent. Filtered, washed with DW and ethanol, and dried at 120 °C for 24 h to produce 60 g of the product's label originally read MBCT.

2.3 Batch absorption procedure

In order to generate a stock solution of AO7 dye (1000 mg/L), 1.0 g of AO7 dye was dissolved in 1 L of DW. This stock solution was then diluted to the required concentrations for the standard calibration curve and absorption experiments. Using batch adsorption investigations, the MBCT's absorption potential, as well as its isotherm and kinetic properties, were identified. With 100 mL of varied AO7 dye solution concentrations (100, 150, 200, 250, and 300 mg/L) and varying doses of MBCT (0.25, 0.50, 0.75, 1.0, and 1.25 g/L) at various at 25 °C, a series of Erlenmeyer flasks (300 mL) were agitated at 200 rpm for a predetermined amount of time. The pH of the solution was adjusted to the proper pH ranges using either 0.1 M HCl or 0.1 M NaOH. By collecting a sample of 0.5 mL of the solution in the Erlenmeyer flask and removing it from the absorbent at different intervals until equilibrium, the concentration of the AO7 dye was considered. The isotherm and kinetic analyses only used the mean values from the three times the adsorption experiments were done. The AO7 dye concentration was measured by spectrophotometry at $\lambda_{max} = 483$ nm. The adsorption capacities at equilibrium (q_e) were predicted by Eq. (1).

$$q_t = \frac{(C_0 - C_t)}{W} \times V \tag{1}$$

where the absorption capacity (q_t) (mg absorbate/g absorbent) is the absorbent's ability to absorb AO7 dye at a certain time from a solution. C_0 (mg/L) is the initial AO7 dye concentration; C_t (mg/L) is the AO7 dye remaining concentration after a specified time. Equation (2) can be applied to compute the removal % of AO7 dye from water.

$$Removal(\%) = \frac{(C_0 - C_t)}{C_0} \times 100 \tag{2}$$

The impact of pH on AO7 dye absorption was investigated by mixing MBCT (0.1 g) with 100 mL of 100 mg/L AO7 dye initial concentration with starting pH values ranging between 2.0 and 12. 0.1 M HCl or NaOH solutions were applied to adjust the pH levels. At 25 °C, the mixture was shaken at 200 rpm for 3 h before being sampled for AO7 dye concentration analysis.

For the isotherm studies, 100 mL of varying initial AO7 dye concentrations of solutions (100, 150, 200, 250, and 300 mg/L) were shaken at 200 rpm for 3 h at 25 °C with various amounts of MBCT (0.25 to 1.25 g/L).

The impact of MBCT dosage and time of contact on AO7 dye absorption was studied by shaking 100 mL of AO7 dye with different MBCT dosages of (0.25, 0.50, 0.75, 1.0, and 1.25 g/L) at various intermission times at 25 °C.

2.4 MBCT characterization

The N_2 adsorption–desorption isotherm on MBCT was measured at the boiling point of N_2 gas using BELSORP-Mini II, BEL Japan, Inc., to calculate the BET surface area (S_{BET}) of the MBCT. This instrument was used to compute the S_{BET} (m²/g), monolayer volume (V_m) (cm³ (STP) g⁻¹), the total volume of pores (p/p_0) (cm³/g), mean diameter of pores (nm), and energy constant (C). Equation (3) can be applied to calculate the average radius of pores (r).

$$r(nm) = \frac{2V_T\left(mLg^{-1}\right)}{a_{s,BET}^{\left(m^2g^{-1}\right)}} \times 1000 \qquad (3)$$

where the V_T (mL/g) is the total pore volume and $a_{S,BET}$ (m²/g) is the calculated specific surface area from BET model analysis. To calculate the surface area of micropores (S_{mi}), surface area of mesopores (S_{mes}), volume of micropores (V_{mi}), and the volume of mesopores (V_{mes}) of MBCT, Barrett-Joyner-Halenda (BJH) model was applied using program software of BELSORP equipment. The size distribution of pores is measured using the BJH model from the desorption isotherm curve.

The MBCT surface morphology was studied using SEM (QUANTA 250) in conjunction with an EDX for elemental analysis. The FTIR (VERTEX70 and ATR unit model V-100) was used to investigate the functional groups on the MBCT surface. The SDT650-Simultaneous Thermal Analyzer device was used to study TGA and DTA at a temperature ranging between 25 and 1000 °C, at a 5 °C/min temperature increase rate.

Author statement for the use of plants In this work, experimental research and field studies on the waste of plants, mandarin orange peels (Citrus reticulata), containing the collection of plant peel waste, comply with relevant institutional, national, and international guidelines and legislation.

3 Results and discussions

3.1 The characteristics of MBCT

To classify the functional groups in the produced MBCT, FTIR analysis was performed. Figure 2 displays the MBCT FT-IR spectrum and the raw mandarin peels (MPs) spectrum. More specifically, the broad absorption peak at 3238.1 cm⁻¹ indicates the existence of the glucose –OH groups and the –NH of the amino groups in the MBCT, whereas the strong peak at 3253.2 cm⁻¹ is specific to the O–H stretching vibration that occurred in MPs. The additional peak showed the addition of the NH_2 group to the MBCT structure. This hypothesis states that the MPs' and
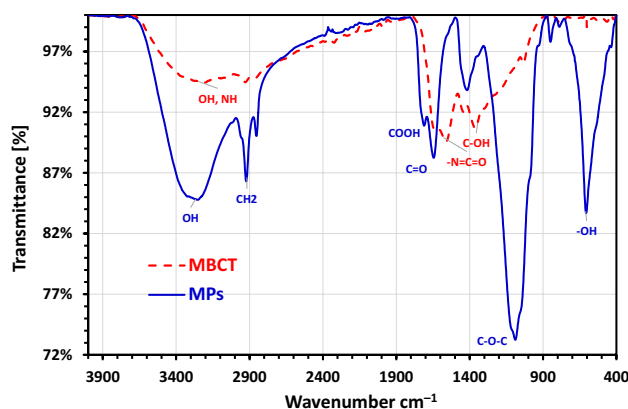

Fig. 2 FTIR analysis of MPs and MBCT adsorbent at wavenumber ranged between 400 and 4000 cm⁻¹

the MBCT's –CH₂ stretching vibrations were present at 2923.3–2854.2 and 299.14–2856.2 cm⁻¹, respectively. It is clear that the C=O stretching of the -COOH group, which was present in MPs but vanished in the produced MBCT, did not occur because there is no absorption band at 1710.3 cm⁻¹ (Fig. 2). Indicating the existence of amide groups in both materials, the bands at 1644.8 cm⁻¹ in MPs and 1635.2 cm⁻¹ in MBCT were present. The frequency of the N–H stretching vibration in the aromatic secondary amine or fatty amine in MBCT was measured at 1563.1 cm⁻¹, suggesting that the N–H functional group in MBCT may have been boosted by the TETA alteration. The strong absorption bands at 1440.3 and 1363.1 cm⁻¹ were attributed to the stretching vibration of the –N=C=O group in MBCT, whereas the absorption band at 1416.9 cm⁻¹ suggests the existence of the C-O groups in MPs. This new band on the MBCT, which was brought on by functional groups having nitrogen, shows that NH and NH_2 groups were successfully introduced after the TETA treatment. The C–O–H functional groups are represented by the band at 1034 cm⁻¹ in MBCT, whereas it is prominent in MPs at 1088.9 cm⁻¹. Additionally, it appears that there was a clear distinction between MPs and MBCT in the band strength range of 1029–1089 cm⁻¹, demonstrating that TETA alteration may have an impact on the C–O–H groups of MBCT (Fig. 2). Additionally, the –OH vibration that showed at 605.8 cm⁻¹ in MPs has completely vanished in the produced MBCT [5, 19, 21].

The BET and BJH models were applied to calculate the MBCT's textural data. The peak of the BET mesopore surface area, the volume of the mesopores, mesopore distribution, total volume of pores, mean diameter of pores, the volume of the monolayer, and specific surface area. MBCT has 1.3521 cm³(STP)/g as a volume of monolayer and 5.98 m²/g as a BET-specific surface area. MBCT had a 11.721 nm mean diameter of pores and 0.018 cm³/g (mesopores) as the total volume of pores. MBCT has a mesopore volume of
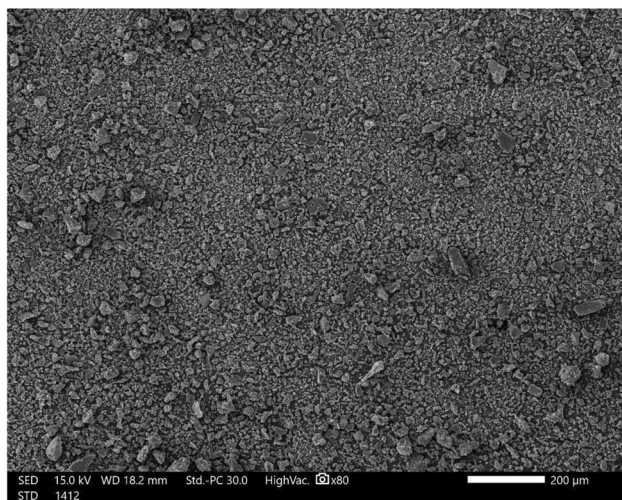
Fig. 3 SEM analysis photo of MBCT at ×80 magnification under high vacuum

Fig. 4 DTA and TGA analyses of the MPs and MBCT in the range between 25 and 1000 °C under 100 mL/min N_2 flow

0.01829 cm^3/g and a mesosurface area of 6.1781 m^2/g. The mesopore distribution peak for MBCT was 1.22 nm. It has been found that the amine functional groups in the created modified activated biomass-based biosorbent constrict the pores [5, 19, 21].

SEM micrographs of the MBCT were examined. According to Fig. 3, which depicts the surface morphology of MBCT, the majority of the pores and caves had been closed by the amine, resulting in active sites. The presence of mesopores and irregular troughs in the biochar surface is visible in Fig. 3. Besides, there are no pores on its surface which is also clear from Fig. 3. A surface amination with TETA may have caused the irregular form, uneven edge aggregation, and nonporous surface that were evident in the image characterization. The decreased surface area determined by the BET analysis could be described by this surface topology [5, 19, 21].

The MBCT underwent an EDX examination to define its chemical make-up. According to reports, the chemical makeup of MBCT has 18.54% sample weight of nitrogen, 51.34% sample weight of carbon, 29.79% sample weight of oxygen atoms, and 18.54% sample weight of nitrogen content. As a result of the method of dehydration with 80% H_2SO_4, a minor amount of sulphur atom (0.33%) was observed.

Figure 4 displays the TGA profile of the MPs and MBCT as a function of temperature for the raw MPs. According to Fig. 4, while the degradation of the MBCT takes place in only two steps, the decomposition of the raw material MPs takes place over the course of four processes. The surface-bound water and moisture in the sample are lost in the 1st step, which takes place between 50 and 150 °C, with weight losses for the raw materials

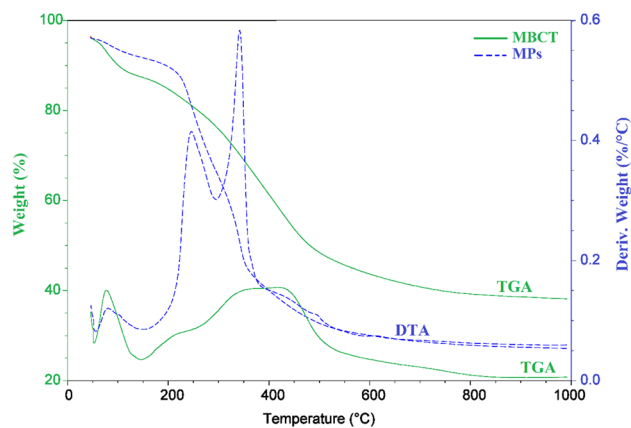MPs and MBCT of 4.5 and 8.85%, respectively. In the 2nd phase of weight loss, MPs lost 25.27% of their body weight between 150 and 300 °C, and MBCT lost 49.33% between 150 and 1000 °C. The MPs lose roughly 25.04% of their weight between 300 and 385 °C in the 3rd mass-loss stage and 14.22% of their weight between 385 and 1000 °C in the 4th and final mass-loss stage [5, 19, 21].

While the determination of phase diagram, measurements of heat change, and various atmospheres decomposition are where differential thermal analysis (DTA) is most frequently utilized, it can also be used purely for identification (Fig. 4). At a flow temperature (Tf: 80.19, 243.82, and 342.32 °C), the MPs sample's DTA curve shows three peaks. However, the MPs' pyrolysis yields three clearly defined deterioration bands. The DTA analysis of the MBCT exposed two distinct degradation bands with good resolution at Tf (77.94 and 416.87 °C) and onset points at 57.2 and 211.68 °C. This established that the MBCT stability was boosted by modification more so than with MPs [5, 19, 21].

The XRD of the MBCT is shown in Fig. 5. The wide peak near $2\theta = 10°–30°$ and $40°–50°$ is denoted by the diffraction peaks in the C (002) and (101) planes, respectively, and it represents an amorphous carbon structure with randomly aligned aromatic sheets. There is a minor peak at $2\theta = 43.669$, which may be related to the existence of some MBCT inorganic components or indicates that the absorbent had an amorphous structure composed of cellulose, hemicellulose, and lignin [5, 19, 21]. The characteristic amorphous biochar peaks, one of the structural components of the primary cell wall of green plants, are detected. However, after sulphonation the intensity of these peaks was reduced. The peaks of residual inorganic phases, such as calcite, quartz, and halite, are visible with a minor peak, $2\theta = 43.669$, after the partial decomposition of organic matter.
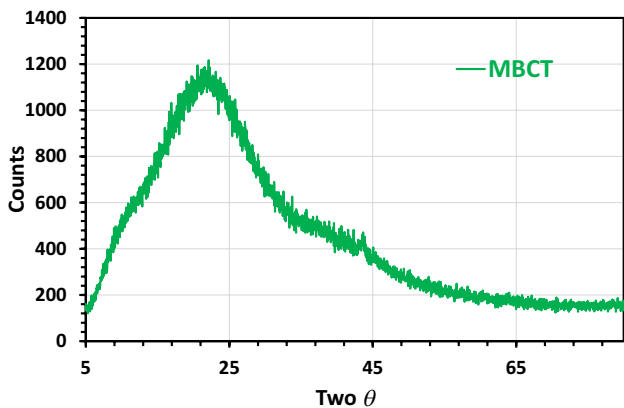
Fig. 5 XRD analysis of MBCT in the 2 Θ range between 5 and 80° at room temperature

3.2 pH Effect on MBCT adsorption

The sorptive uptake of sorbate molecules is impacted by the system pH owing to the absorbent (MBCT) surface properties and the sorbate (dye) molecule's ionization or dissociation [22]. The point of zero charges (pH_{PZC}), according to Fig. 6a, was found to be 10.17. pH below the pH_{PZC}, sites on the sorbent surface were positively charged, and pH above the pH_{PZC}, the sites on the sorbent surface were negatively charged [5, 19, 21]. The impact of pH on the absorption of AO7 dye to MBCT is shown in Fig. 6b, which showed a decrease in the percentage (%) of AO7 dye molecules sorbed to MBCT as the system pH was improved from pH 2–10. The optimum dye sorption being studied was observed at pH 2, which could be ascribed to the electrostatic interaction between the positively charged surface sites on the MBCT (protonation of sorbent sites-H^+) and the negatively charged anionic dye molecules. With further increase in the system

pH, a reduction in the % of AO7 dye molecules absorbed to the absorbent was noticed due to the deprotonation of the sites on the MBCT (OH^-), which led to the electrostatic repulsion between the negatively charged sites on the MBCT surface and the negatively charged anionic AO7 dye molecules. Findings from the present study are in line with the findings [11, 23–25].

3.3 Impact of MBCT dose

To improve the dosage of sorbent utilized for the confiscation of AO7 dye molecules, sorption studies were assessed with varying sorbent dosages of 0.25–1.25 g/L (Fig. 7). It was noticed that dye molecule uptakes in % to the MBCT sorbent were improved with rising sorbent dosage as time was improved. This phenomenon was ascribed to the absorbent's improved surface area,
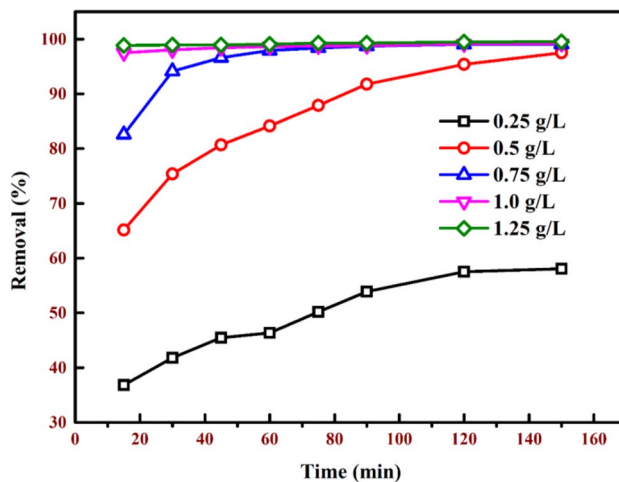

Fig. 7 The plot of the influence of sorbent dose on the sorption AO7 dye to MBCT 0.25 to 1.25 g/L doses and 100 mg/L initial dye concentration
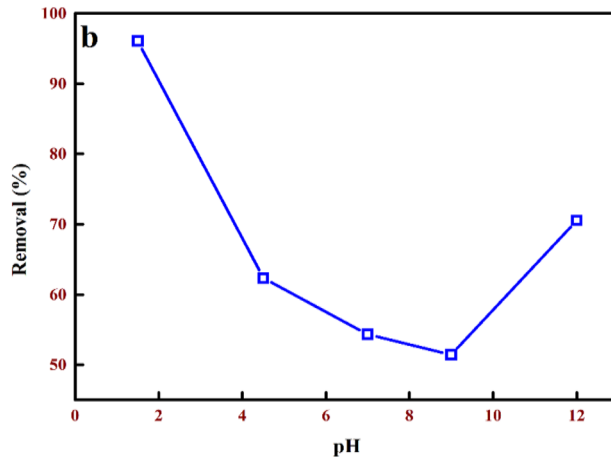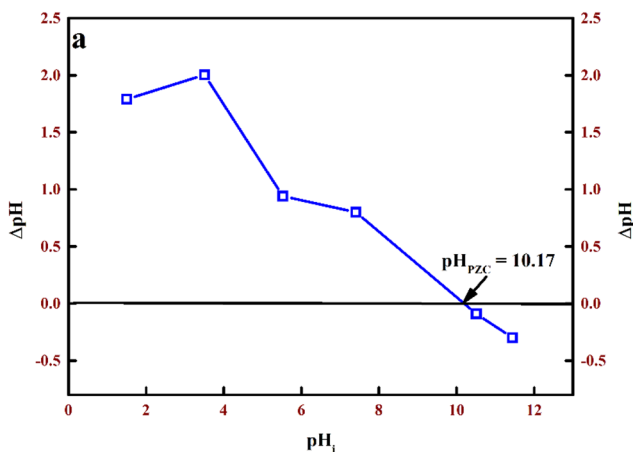

Fig. 6 Plots of **a** pH_f-pH_i against pH_i with the assessed pH_{PZC} of MB-CT and **b** the pH impact on the sorption of AO7 dye using pH ranged between 2 and 12 at room temperature
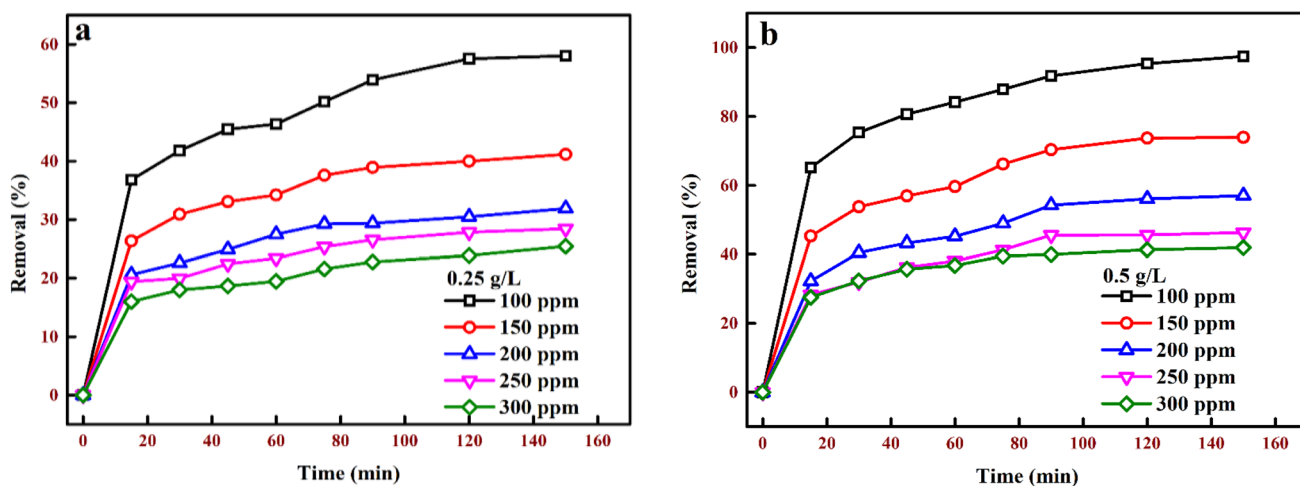
Fig. 8 The plots of initial dye concentration on the absorption process of AO7 dye molecules of 100–300 mg/L initial dye concentration to **a** 0.25 g/L of MBCT sorbent and **b** 0.50 g/L of MBCT sorbent

which led to the increased available active sites on the MBCT surface for dye molecules sorption. After 20 min, saturation in the % of dye molecules confiscated was noticed for sorbent doses used (1.25 g/L), and this was also attributed to particles accumulation ensuing in a reduction in the total surface area of available sorbent for the dye molecules sorption [23, 24].
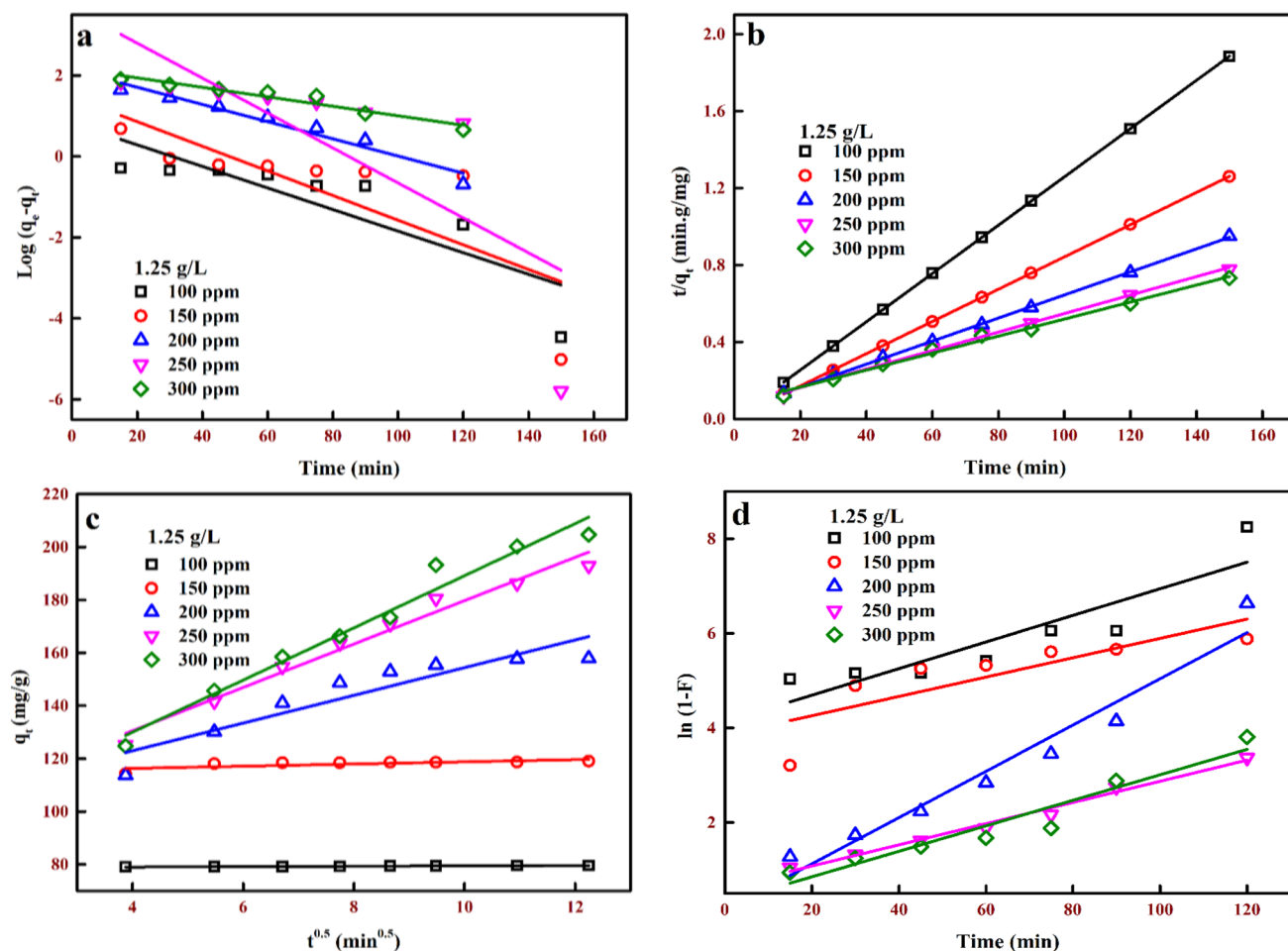

Fig. 9 Plots of **a** PFOR, **b** PSOR, **c** IND, and **d** FD models using 100–300 mg/L initial dye concentration and 1.25 g/L adsorbent dose

Table 1 Measured PFOR and PSOR model data using 0.25–1.25 g/L adsorbent doses and 100–300 mg/L initial dye concentration at room temperature

Parameter			PFOR model			PSOR model			
MBCT dose (g/L)	AO7 dye (mg/L)	q_e (exp.)	q_e (calc.)	k_1	R^2	q_e (calc.)	$k_2 \times 10^3$	h	R^2
0.25	100	232.19	211.35	32.47	0.857	256.41	0.23	15,175	0.993
	150	246.97	192.62	31.32	0.946	270.27	0.26	19,305.0	0.998
	200	255.23	1665.71	72.77	0.628	277.78	0.25	19,193.9	0.997
	250	265.35	182.56	26.02	0.945	312.50	0.21	20,408.2	0.995
	300	305.10	163.38	17.50	0.965	333.33	0.16	18,148.8	0.990
0.5	100	194.98	2237.18	87.28	0.629	208.33	0.40	17,271.2	0.998
	150	221.74	258.82	40.07	0.864	250.00	0.23	14,556.0	0.995
	200	228.15	1764.82	74.39	0.708	256.41	0.20	13,297.9	0.994
	250	231.35	1574.35	76.00	0.745	256.41	0.23	15,197.6	0.995
	300	251.37	3049.30	91.43	0.654	270.27	0.33	24,096.4	0.999
0.75	100	132.09	514.40	112.16	0.860	135.14	3.15	57,471.3	1.000
	150	195.17	3028.31	93.73	0.637	212.77	0.37	16,750.4	0.999
	200	213.15	152.62	26.71	0.948	238.10	4.20	238,095.2	0.996
	250	226.15	3566.97	88.20	0.605	250.00	0.23	14,144.3	0.996
	300	236.85	241.66	37.31	0.906	263.16	0.23	16,025.6	0.995
1.0	100	99.17	1.35	14.28	0.254	99.01	24.29	238,095.2	1.000
	150	148.76	24.61	35.70	0.924	151.52	2.77	63,694.3	1.000
	200	194.82	133.14	30.63	0.971	212.77	0.35	16,000.0	0.998
	250	211.54	133.14	24.41	0.958	232.56	0.26	14,164.3	0.997
	300	220.39	206.68	33.62	0.966	243.90	0.24	14,409.2	0.997
1.25	100	79.61	1.28	28.10	0.812	80.00	50.40	322,580.6	1.000
	150	119.05	29.38	70.01	0.623	119.05	18.09	256,410.3	1.000
	200	157.93	72.56	36.16	0.838	166.67	0.80	22,271.7	1.000
	250	192.94	4593.04	99.49	0.589	208.33	0.34	14,881.0	0.998
	300	204.70	192.44	32.01	0.945	227.27	0.25	12,987.0	0.994

3.4 Impact of AO7 dye preliminary concentration

A critical factor that impacts dye sorption using nano-sorbents is the initial sorbate concentration, as it controls the sorbent capacity for certain constituents of initial sorbate concentration. Typically, the sorption capacity and % removals are directly and indirectly associated with the dye concentration; the sorption capacity and % removal increase and decrease with an improved initial concentration of dye [3, 26]. Dye initial concentration directly impacts dye confiscation effectiveness by decreasing or increasing the accessibility of binding sites on the sorbent surface [27]. Depending on the direct correlation between the dye concentration and the availability of binding sites on the sorbent's surface, the initial dye concentration factor has varying effects. As shown in Fig. 8, as the interaction time is lengthened, the percentage of AO7 dye molecules confined to the sorbent sites decreases with increasing starting dye concentrations. At low concentrations, improved confiscation was due to vacant functional sites on the absorbent surface, and with an increase in initial dye concentration, the amount of available active sites for dye sorption was deficient, hence the reduced

confiscation of dye molecules at higher initial concentrations [26–28].

3.5 Kinetic models

The sorption kinetics relies on the sorbent-sorbate interaction and system conditions and has been studied for their water contamination management application suitability. Two critical assessment elements for a sorption process procedure unit are the rate of reaction and the mechanism. The solute rate of uptake defines the residence time needed for achieving the sorption reaction and can be specified from kinetic evaluation. The rate of sorption is a vital reason for an improved variety of materials to be employed as a sorbent, where the sorbent must have a substantial sorption capacity and a fast sorption rate [26]. The kinetic models employed were the PFOR, PSOR, IND, and FD, with the various plots of these models in linear forms which are shown in Fig. 9. According to the determined parameters in Table 1 and Table 2, the PSOR model best fitted the working data owing to the ultimate value of linear regression coefficient (R^2) obtained (> 0.99). The

Table 2 Measured parameters of IND and FD models using 0.25–1.25 g/L adsorbent doses and 100–300 mg/L initial dye concentration at room temperature

MBCT dose (g/L)	AO7 dye (mg/L)	IND model			FD model	
		K_{dif}	C	R^2	K_{FD}	R^2
0.25	100	10.719	107.730	0.977	0.032	0.857
	150	10.686	124.640	0.957	0.025	0.978
	200	11.189	125.480	0.954	0.021	0.976
	250	12.125	143.050	0.968	0.139	0.544
	300	13.726	136.900	0.982	0.017	0.965
0.50	100	7.652	107.160	0.966	0.045	0.830
	150	10.848	99.111	0.958	0.025	0.976
	200	12.052	90.671	0.956	0.031	0.927
	250	11.688	100.680	0.938	0.036	0.876
	300	10.155	138.620	0.919	0.030	0.986
0.75	100	2.125	110.440	0.632	0.050	0.983
	150	8.104	103.540	0.954	0.028	0.976
	200	10.615	91.507	0.962	0.027	0.948
	250	11.265	95.613	0.960	0.037	0.906
	300	11.592	106.570	0.947	0.022	0.923
1.00	100	0.196	96.970	0.930	0.035	0.861
	150	2.292	125.010	0.690	0.036	0.924
	200	8.178	101.620	0.964	0.027	0.977
	250	10.121	95.033	0.963	0.024	0.958
	300	11.074	95.375	0.954	0.031	0.946
1.25	100	0.070	78.763	0.936	0.028	0.812
	150	0.412	114.680	0.540	0.020	0.670
	200	5.234	102.050	0.861	0.049	0.953
	250	8.194	97.778	0.977	0.022	0.988
	300	9.856	90.574	0.971	0.027	0.930

determined q_e (mg/g) values from both experimental and calculated were very close according to the PSOR model, which authenticates this model's suitability to describe the absorption process of AO7 dye to MBCT. While rate-defining steps and diffusion did not control the IND and FD linear plots through liquid film bordering the sorbent, as the linear plots did not go via the origin of their various plots. Also, the R^2 values of both the IND and FD models were comparatively low compared to that of the PSOR model. Thus, the absorption process of AO7 dye to MBCT
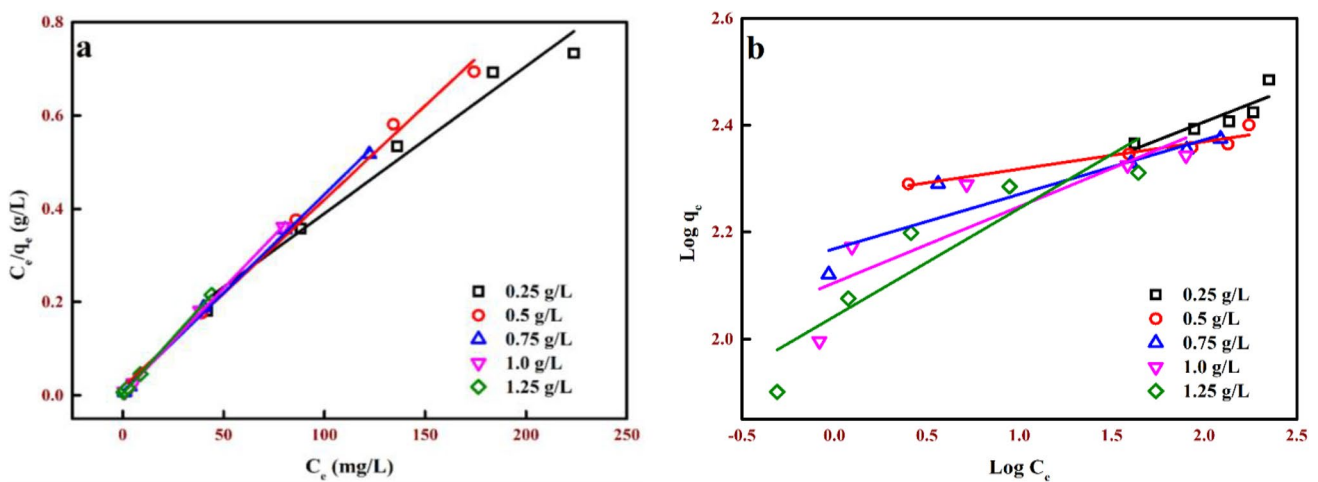

Fig. 10 The plots **a** LNR and **b** FRH models using 0.25–1.25 g/L adsorbent doses and 100 mg/L initial dye concentration at room temperature

Table 3 Measured data of LNR and FRH models using 0.25–1.25 g/L adsorbent doses and 100–300 mg/L initial dye concentration at room temperature

Isotherm Model	Isotherm data	MBCT dose				
		0.25 g/L	0.50 g/L	0.75 g/L	1.0 g/L	1.25 g/L
LNR	Q_m (mg/g)	312.50	250.00	238.10	222.22	208.33
	$b \times 10^3$	0.04	0.24	0.51	1.05	1.23
	R^2	0.976	0.995	0.999	1.000	1.000
FRH	$1/n$	0.1353	0.0513	0.1019	0.1424	0.202
	$K_a \times 10^3$	136.62	184.80	147.54	127.47	110.26
	R^2	0.779	0.913	0.847	0.756	0.838

sorbent was based on the assumption of chemisorption involving valency force via sharing or exchange of electrons between the MBCT and AO7 dye molecules [7, 24].

3.6 Isotherm models

The equilibrium state of the absorption process is measured by the diffusion of dye molecules between the absorbent and the liquid phase, which one or more isotherm models often explain. For the design process application, isotherm data can precisely be fitted into various isotherm models to find an appropriate model [24]. In this present study, the LNR and FRH models were utilized. The linear plot of the different models is shown in Fig. 10. The measured parameter assessed from the fittings employing the different models is shown in Table 3. The assessed R^2 values for the LNR model perfectly described the absorption process of AO7 dye to MBCT, which was due to the equivalent and identical dye molecules distributed over the porous sorbent surface. The calculated dimensionless separation factor (R_L) was within 0.0081–0.189, which presented that the absorption process was favourable when $0 < R_L < 1$. The assessed absorption capacity was 312.50 mg/g using 0.25 g/L of the MBCT. In comparing of the absorption capacities of various absorbents employed to confiscate of AO7 dye (Table 4), it is obvious that MBCT absorbent was more efficient in eliminating of AO7 dye molecules.

Table 4 Comparison of various sorbent sorption capacities employed for AO7 dye confiscation

Nanomaterial	Q_m (mg/g)	References
MBCT	312.50	Present study
Spherical-shaped nanocarbons	185.18	[29]
Canola stalks biosorbent	25.06	[24]
Treated bagasse	144.93	[30]
Kenya tea pulps	31.25	[11]
Magnetic graphene/chitosan	42.70	[23]
AC from deinked pulp waste sludge	12.88	[31]
Polypyrrole/nanosilica composite	181.40	[13]

3.7 Regeneration study

0.1 M NaOH and HCl completed desorption studies of the AO7 dye from the MBCT adsorbent as an elution media to study the viability and MBCT reusability for the absorption of AO7 dye. In this study, the percentage of AO7 dye desorption decayed with the regeneration cycles increased (Fig. 11). Six cycles of absorption/desorption have been studied using the regenerating MBCT. The change in adsorption and desorption remained mainly near constant throughout the cycles. However after six cycles, it had decreased by about 6%. It suggests it could be used as a durable AO7 dye removal from water (Fig. 11).

4 Conclusion

This research investigation showed that MPs wastes, which are agricultural wastes, may be used to create an affordable, effective, and ecologically friendly adsorption material. The dried MPs were treated with 80% H_2SO_4 at 200 °C, then oxidized with H_2O_2, and finally aminated
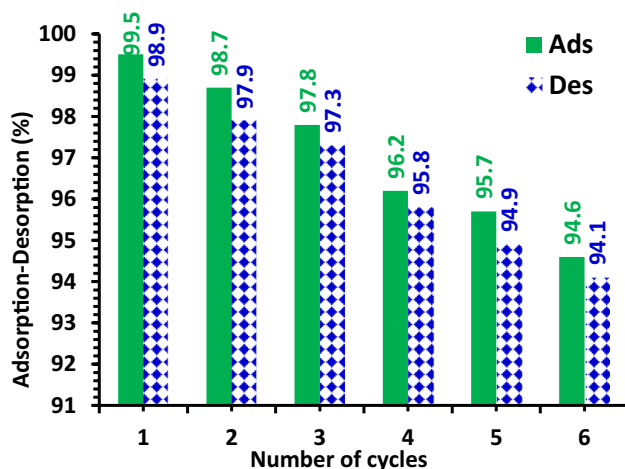
Fig. 11 Regeneration study of AO7 dye adsorption–desorption by MBCT using 1.25 g/L adsorbent dose and 100 mg/L initial dye concentration at room temperature

by treatment with TETA in order to produce MBCT for application in the absorption of AO7 dye, an azo dye. It is observed that the mass of adsorbent used, the initial concentration, the duration of the contact time, and the pH level of the aqueous solution all affect how much AO7 dye is ingested. The optimal pH for MBCT to adsorb the AO7 dye was found to be 2.0 using MBCT as a model. Biochars utilize multiple physical–chemical interactions for adsorption; thus, dyes from various classes can be removed from wastewater solutions. Since each dye has a unique chemical structure, the chemistry of the compound can be used to determine the degree of adsorption by biochar. The point of zero charges (pH_{PZC}) was found to be 10.17. pH below the pH_{PZC}, sites on the sorbent surface were positively charged, and pH above the pH_{PZC}, the sites on the sorbent surface were negatively charged. The best removal of AO7 dye was 99.07% using an initial concentration of 100 mg/L of AO7 dye and a 0.75 g/L MBCT. The Q_m predicted for the MBCT was 312.50 mg/g, using 0.75 g/L of the sorbent. The LNR and PSOR were best suited to define the experimental MBCT data. The results indicate that the manufactured MBCT adsorbent may be useful for removing the AO7 dye from the aquatic environment. This again opens the door to using MBCT, which has the extra virtue of being ecologically friendly, as an applicable absorbent for absorbing the AO7 dye from aquatic environments.

Data availability The datasets used in this investigation are accessible for review upon request from the corresponding author of the paper.

Declarations

Consent to participate Consent to participate is not applicable.

Competing interests The authors declare no competing interests.

References

1. Ukhurebor KE, Aigbe UO, Onyancha RB, Nwankwo W, Osibote OA, Paumo HK, Ama OM, Adetunji CO, Siloko IU (2021) Effect of hexavalent chromium on the environment and removal techniques: a review. J Environ Manag 280:111809

2. Sudarni DHA, Aigbe UO, Ukhurebor KE, Onyancha RB, Kusuma HS, Darmokoesoemo H, Osibote OA, Balogun VA, Widyaningrum BA (2021) Malachite green removal by activated potassium hydroxide clove leaves agro-waste biosorbent: characterization, kinetics, isotherms and thermodynamics studies. Ads Sci Tech 1145312:1–15

3. Zhang K, Yi Y, Fang Z (2022) Remediation of cadmium or arsenic contaminated water and soil by modified biochar a review Chemosphere 136914

4. Song J, Zhang S, Li G, Du Q, Yang F (2020) Preparation of montmorillonite modified biochar with various temperatures and their mechanism for Zn ion removal. J Hazard Mater 391:121692

5. Eldeeb TM, Aigbe UO, Ukhurebor KE, Onyancha RB, El-Nemr MA, Hassaan MA, Osibote OA, Ragab S, Okundaye B, Balogun VA, El Nemr A (2022) Biosorption of acid brown 14 dye to mandarin-biochar-CO-TETA derived from mandarin peels. Biomass Convers Biorefine 2022:1–21

6. Adar E (2021) Removal of acid yellow 17 from textile wastewater by adsorption and heterogeneous persulfate oxidation. Int J Environ Sci Technol 18:483–498

7. Chahinez HO, Abdelkader O, Leila Y, Tran HN (2020) One-stage preparation of palm petiole-derived biochar: characterization and application for adsorption of crystal violet dye in water. Environ Tech Innovat 19:100872

8. Kerie E, Alemu A (2022) Removal of acid yellow dye 17 from aqueous solutions using an activated bone char. Water Quality Res J 57(4):278–290

9. Biglari H, Afsharnia M, Javan N, Phenol SA (2016) removal from aqueous environment by adsorption onto activated carbon of Meswak's root treated with KMnO4. Iran J Heal Sci 4(1):20–30

10. Khandan M, Eyni Z, Ataei manesh L, Khosravi Z, Biglari H, Koohpaei A, et al (2016) Relationship between musculoskeletal disorders and job performance among nurses and nursing aides in main educational hospital in Qom province, 2014. Res J Med Sci 10(4):307–312

11. Naraghi B, Zabihi F, Narooie MR, Saeidi M, Biglari H (2017) Removal of acid orange 7 dye from aqueous solutions by adsorption onto Kenya tea pulps; granulated shape. Electron Physician 9(5):4312–4321

12. Saghir S, Pu C, Fu E, Wang Y, Xiao Z (2022) Synthesis of high surface area porous biochar obtained from pistachio shells for the efficient adsorption of organic dyes from polluted water. Surfaces and Interfaces 34:102357

13. Sillanpää M, Mahvi AH, Balarak D, Khatibi AD (2021) Adsorption of acid orange 7 dyes from aqueous solution using polypyrrole/nanosilica composite: experimental and modelling. Inter J Environ Anal Chem. https://doi.org/10.1080/03067319.2020.1855338

14. Ennouri R, Panizza M, Mhiri T, Elaoud SC (2017) Electrochemical behaviour of acid orange 7 by cyclic voltammetry in different solvents. Port Electrochim Acta 35(5):269–277

15. Yarmohammadi H, Poursadeghiyan M, Shorabi Y, Ebrahimi MH, Rezaei G, Biglari H et al (2016) Risk assessment in a wheat winnowing factory based on ET and BA method 11(3):334–338

16. Mirzabeygi M, Naji M, Yousefi N, Shams M, Biglari H, Mahvi AH (2016) Evaluation of corrosion and scaling tendency indices in water distribution system: a case study of Torbat Heydariye. Iran Desalination and Water Treatment 57(54):25918–32526

17. Xin Q, Fu J, Chen Z, Liu S, Yan Y, Zhang J et al (2015) Polypyrrole nanofibers as a high-efficient adsorbent for the removal of methyl orange from aqueous solution. J Environ Chem Eng 3(3):1637–1647

18. Blanchard R, Mekonnen TH (2022) Synchronous pyrolysis and activation of poly (ethylene terephthalate) for the generation of activated carbon for dye contaminated wastewater treatment. J Environ Chem Eng 10(6):108810

19. Nguyen XC, Nguyen TTH, Nguyen THC, Van Le Q, Vo TYB, Tran TCP, La DD, Kumar G, Nguyen VK, Chang SW, Chung WJ (2021) Sustainable carbonaceous biochar adsorbents derived from agro-wastes and invasive plants for cation dye adsorption from water. Chemosphere 282:131009

20. Koyuncu F, Güzel F, Sayğılı H (2018) Role of optimization parameters in the production of nanoporous carbon from mandarin shells by microwave-assisted chemical activation and utilization as dye adsorbent. Adv Powder Technol 29(9):2108–2118

21. Yılmaz M, Eldeeb TM, Hassaan MA, El-Nemr MA, Ragab S, El Nemr A (2022) The use of mandarin-biochar-O$_3$-TETA (MBT) produced from mandarin peels as a natural adsorbent for the removal of acid red 35 (AR35) dye from water. Environ Proces 9:44. https://doi.org/10.1007/s40710-022-00592-w

22. Alemu A, Kerie E (2022) Removal of acid yellow 17 dye from aqueous solutions using activated water hyacinth (Eichhornia crassipes). Water Practice Technol 17(6):1294–1304

23. Sheshmani S, Ashori A, Hasanzadeh S (2014) Removal of acid orange 7 from aqueous solution using magnetic graphene/chitosan: a promising nano-adsorbent. Inter J Biol Macromol 68:218–224

24. Hamzeh Y, Ashori A, Azadeh E, Abdulkhani A (2012) Removal of acid orange 7 and remazol black 5 reactive dyes from aqueous solutions using a novel biosorbent. Mater Sci Eng C 32(6):1394–1400

25. Eleryan A, Yılmaz M, El-Nemr MA, Ragab S, Helal M, Hassaan MA, El Nemr A (2022) Mandarin Biochar-TETA (MBT) prepared from Citrus reticulata peels for adsorption of acid yellow 11 dye from water. Sci Rep 12:17797

26. Bharathi KS, Ramesh ST (2013) Removal of dyes using agricultural waste as low-cost adsorbents: a review. Appl Water Sci 3(4):773–790

27. Rápó E, Tonk S (2021) Factors affecting synthetic dye adsorption; desorption studies: a review of results from the last five years (2017–2021). Molecules 26(17):5419

28. Goswami R, Dey AK (2022) Synthesis and application of treated activated carbon for cationic dye removal from modelled aqueous solution. Arab J Chem 15(11):104290

29. Krishnappa B, Mannekote Shivanna J, Naik M, Padova PD, Hegde G (2021) Acid Orange-7 uptake on spherical-shaped nanocarbons. Nanomaterials and Nanotechnology 11:18479804211055030. https://doi.org/10.1177/18479804211055031

30. Malek NANN, Sihat NM, Khalifa MA, Kamaru AA, Sani NS 2016 Adsorption of acid orange 7 by cetylpyridinium bromide modified sugarcane bagasse J Teknologi 78 1–2

31. Rajeshkanna P, Nagarajan NS, Meenakshi S (2018) Rhodamine B and acid orange 7 adsorption onto activated carbon from deinked pulp waste sludge: adsorption and kinetics studies. Environ Sci 14(1):169

Authors and Affiliations

Ahmed Eleryan[1] · Mohamed A. Hassaan[1] · Uyiosa O. Aigbe[2] · Kingsley E. Ukhurebor[3] · Robert B. Onyancha[4] · Mohamed A. El-Nemr[5] · Safaa Ragab[1] · Ismail Hossain[6] · Ahmed El Nemr[1] 🔵

Ahmed Eleryan
aeleryan71@yahoo.com

Mohamed A. Hassaan
mhss95@mail.com

Uyiosa O. Aigbe
uyi4we@gmail.com

Kingsley E. Ukhurebor
ukeghonghon@gmail.com

Robert B. Onyancha
08muma@gmail.com

Mohamed A. El-Nemr
mohamedelnemr1992@yahoo.com

Safaa Ragab
safaa_ragab65@yahoo.com

Ismail Hossain
hossain.ismail44@yahoo.com

1. Environment Division, National Institute of Oceanography and Fisheries (NIOF), Kayet Bey, Elanfoushy, Alexandria, Egypt

2. Department of Mathematics and Physics, Faculty of Applied Sciences, Cape Peninsula University of Technology, Cape Town, South Africa

3. Department of Physics, Faculty of Science, Edo State University Uzairue, Edo State, Nigeria

4. Department of Technical and Applied Physics, School of Physics and Earth Sciences Technology, Technical University of Kenya, Nairobi, Kenya

5. Department of Chemical Engineering, Faculty of Engineering, Minia University, Minia, Egypt

6. School of Natural Sciences and Mathematics, Ural Federal University, Yekaterinburg 620000, Russia